RESEARCH ARTICLE

ADVANCED
ENERGY & SUSTAINABILITY
RESEARCH
Open Access

www.advenergysustres.com

Green Inks for the Fabrication of Organic Solar Cells: A Case Study on PBDTTPD:PC$_{61}$BM Bulk Heterojunctions

Christian Sprau, Ana Milena Cruz, Lorenzo Bautista, Laura Molina, Michael Wagner, Christos L. Chochos, Mónica Della Pirriera, and Alexander Colsmann*

Nonhalogenated ecofriendly solvents are an important asset to avoid costly safety precautions during the fabrication of organic solar cells by printing. Yet, in the past, the quest for suitable nontoxic solvents has widely used empirical approaches. Herein, a comprehensive solubility study is rolled out embracing Hansen solubility parameters (HSPs), tailoring of binary solvents and rational choices of solvent additives, identifying ecofriendly solvents or solvent combinations for the deposition of poly-benzodithophene-thienopyrroledione (PBDTTPD)/fullerene thin-film blends. A particular challenge is the low polymer solubility even in common halogenated solvents. Following the HSPs, initially, a list of suitable solvent candidates is identified which are tested toward their applicability in solar cell fabrication. Among the shortlisted solvents, significant differences between *p*-xylene and *o*-xylene are observed, which can be compensated using solvent additives. The ecofriendly green solvent eucalyptol in combination with benzaldehyde and *p*-anisaldehyde in a ternary solvent mixture gives rise to decent solar cell performances. Solar cells are produced with power conversion efficiencies matching those conventionally fabricated from state-of-the-art halogenated solvents comprising chlorobenzene and chloronaphthalene. Notably, the Hansen solubility approach provides an initial choice of solvents, but comes to its limits in predicting the best micromorphology formation, or if solvents react with the organic semiconductors.

1. Introduction

Due to their mechanical flexibility, free-form design, and light weight, organic solar cells (OSCs) can address various new markets. OSCs have the potential to become a fully sustainable and "green" technology, as the organic macromolecules usually omit any toxic or rare elements. Fabrication by large-area printing and coating from semiconductor solutions is widely considered to reduce the production costs and the production energy consumption, the latter adding to the sustainability of the technology.[1–3] On laboratory scale, today's solution-processable OSCs achieve power conversion efficiencies (PCEs) of more than 11% based on polymer:fullerene,[4,5] and exceeding 17% based on recent nonfullerene acceptors,[6,7] yet fullerenes often remain first choice when targeting large-scale fabrication and pilot applications.[8,9]

The basic working principle of organic light-harvesting layers relies on bulk heterojunctions, which comprise an interpenetrating network of two (or more) organic semiconductors, one of which is an electron donor, whereas the other one accepts electrons. The blend morphology of the bulk heterojunction is decisive for the performance of the OSCs. It forms during the deposition and drying of a semiconductor ink, that is, π-conjugated organic molecules in a

Dr. C. Sprau, Prof. A. Colsmann
Material Research Center for Energy Systems (MZE)
Karlsruhe Institute of Technology (KIT)
Strasse am Forum 7, 76131 Karlsruhe, Germany
E-mail: alexander.colsmann@kit.edu

Dr. C. Sprau, M. Wagner, Prof. A. Colsmann
Light Technology Institute
Karlsruhe Institute of Technology (KIT)
Engesserstrasse 13, 76131 Karlsruhe, Germany

Dr. A. M. Cruz, Dr. L. Bautista, L. Molina, Dr. M. Della Pirriera
Leitat Technological Center
c/ de la Innovació 2, 08225 Terrassa, Spain

Dr. C. L. Chochos
Advent Technologies SA
Patras Science Park, Stadiou Street, Platani-Rio, 26504 Patra, Greece

Dr. C. L. Chochos
Institute of Chemical Biology
National Hellenic Research Foundation
48 Vassileos Constantinou Avenue, Athens 11635, Greece

**ADVANCED
SCIENCE NEWS**

www.advancedsciencenews.com

**ADVANCED
ENERGY & SUSTAINABILITY
RESEARCH**
Open Access

www.advenergysustres.com

solvent or solvent mixture. Any suitable solvent must 1) provide sufficient semiconductor solubility, 2) have rheological properties and drying kinetics suitable for printing, and 3) promote the formation of a favorable blend morphology. On lab scale, most standard solvents are halogenated, such as chlorobenzene, dichlorobenzene, or chloroform. However, in countries with a strict environmental, health and safety (EHS) legislation, the related safety precautions and solvent vapor capturing would incur significant additional device production costs. The replacement of halogenated solvents by less toxic, nonhalogenated alternatives, would therefore facilitate the uptake of this young technology by industry, and eventually these "green inks" should also comprise organic semiconductors that were synthesized avoiding toxic compounds.[10,11] Notably, not every nonhalogenated solvent can be considered "green," as the overall environmental impact of solvents depends on many aspects, such as emission and use of resources over the full life-cycle as well as substance hazards and regulatory measures, which may even vary from country to country.[12,13] Although nonhalogenated solvents were used to produce solar cells with high PCEs,[4,5,14–27] in most studies, the solvents were chosen following a trial-and-error approach or educated guessing.

A more systematic approach to select suitable solvents or solvent mixtures from the variety of organic solvents uses the Hansen solubility parameters (HSPs).[28,29] The HSPs are an advancement of the total Hildebrand parameter δ_T which was originally introduced by Hildebrand and Scott to provide a numerical estimate of the degree of interaction between materials:[30]

$$\delta_T = \sqrt{\frac{E}{V}} \tag{1}$$

where V is the molar volume and $E = \Delta H - RT$ is the total cohesion energy which depends on the latent heat of vaporization ΔH and the inner energy RT, with T representing the absolute temperature, and R the global ideal gas constant. E is the energy that is required to evaporate the liquid and thus to separate all solvent molecules by overcoming intermolecular attraction (cohesion). In the Hildebrand theory, based on nonpolar hydrocarbon solvents and not including hydrogen bonding, materials with similar δ_T are miscible, whereas large differences in δ_T reflect immiscibility. Hansen advanced the Hildebrand parameter by splitting δ_T into three different contributions from nonpolar atomic dispersive (δ_D), permanent dipolar (δ_P), and molecular hydrogen bonding (δ_H) interactions between (solvent) molecules[31]

$$(\delta_T)^2 = (\delta_D)^2 + (\delta_P)^2 + (\delta_H)^2 \tag{2}$$

Each solvent can then be described by the parameter triple (δ_D, δ_P, δ_H), the HSPs, which is best visualized in a 3D coordinate system, the Hansen space. A second material with HSPs of ($\delta_{D,2}$, $\delta_{P,2}$, $\delta_{H,2}$) is miscible with a solvent at the coordinates ($\delta_{D,1}$, $\delta_{P,1}$, $\delta_{H,1}$) if the solubility parameter distance

$$R_a = \sqrt{4 \cdot (\delta_{D,2} - \delta_{D,1})^2 + (\delta_{P,2} - \delta_{P,1})^2 + (\delta_{H,2} - \delta_{H,1})^2} \tag{3}$$

of their HSPs is sufficiently small. Experiments have shown that dispersive energy differences in general have a stronger impact on solubility, which is why they are empirically weighed with the factor 4.[31]

Solvents that dissolve a certain material, e.g., a polymer, possess a sufficiently small solubility parameter distance to the polymer. As such, they are located within a spheroidal volume in the Hansen space of which the surface coordinates have the same solubility distance R_0 to the HSPs of the polymer. By scaling of the δ_D axis with the factor 4, spheroids are conveniently transformed into spheres ("Hansen spheres"). Solvents outside the sphere are unlikely to dissolve the polymer and hence are considered "poor."

In the past, the experimental determination of HSPs to identify suitable solvents for bulk heterojunction compounds was successfully applied to polymers,[28,32–34] oligomer donors,[29,32] and the fullerene acceptors [6,6]-phenyl C$_{61}$-butyric acid methyl ester (PC$_{61}$BM) and [6,6]-phenyl C$_{71}$-butyric acid methyl ester (PC$_{71}$BM).[28,29,32] In these earlier reports, the Hansen spheres were determined by investigating the solubility of the components in more than 30 different reference solvents. The Hansen sphere determination was advanced by Machui et al. using a binary solvent gradient method,[35,36] in which one good solvent is mixed with (at least) three different poor cosolvents. The gradient of solvent ratios then follows straight lines in the Hansen space. After analyzing the solubility of a solute in these binary solvent/cosolvent mixtures, the Hansen sphere can be fitted around good solvent mixtures. Using this approach, the experimental effort is significantly reduced, whereas the accuracy of the Hansen sphere determination is enhanced.[35]

In this work, we used the binary solvent gradient method to calculate the HSP of a polymer:fullerene blend comprising poly (di(2-ethylhexyloxy)benzo[1,2-b:4,5-b']dithiophene-alt-octylthieno [3,4-c]pyrrole-4,6-dione) (PBDTTPD) and PC$_{61}$BM (**Figure 1**a). In contrast to most of the earlier reports, we limited the choice of solvents to green solvents and challenged the Hansen approach using the polymer PBDTTPD which is known to be poorly soluble even in common halogenated solvents, but which derives its benefits from scalability due to the low synthetic complexity and optional green synthesis by direct arylation.[37–39] However, because of its generally low solubility, PBDTTPD was reported to form best morphologies from hot chlorobenzene solutions (at least 115 °C) which would not be compatible with any industrially relevant deposition technique.[40,41] Out of a database of 1239 solvents (HSPiP 4.1.04 software), we found some nonhalogenated solvents within the solubility spheres that comply with a strict list of solvent requirements including evaporation and toxicity criteria. These solvents were then investigated toward their applicability for the deposition of light-harvesting PBDTTPD: PC$_{61}$BM thin films.

2. Results and Discussions

2.1. Study of HSPs

To find solvents that are suitable to dissolve PBDTTPD:PC$_{61}$BM blends, the individual HSPs of both components were determined using the binary solvent gradient method. PBDTTPD was synthesized yielding an average molecular weight $\overline{M}_n = 19 \text{ kg mol}^{-1}$. For comparison, the HSPs of other
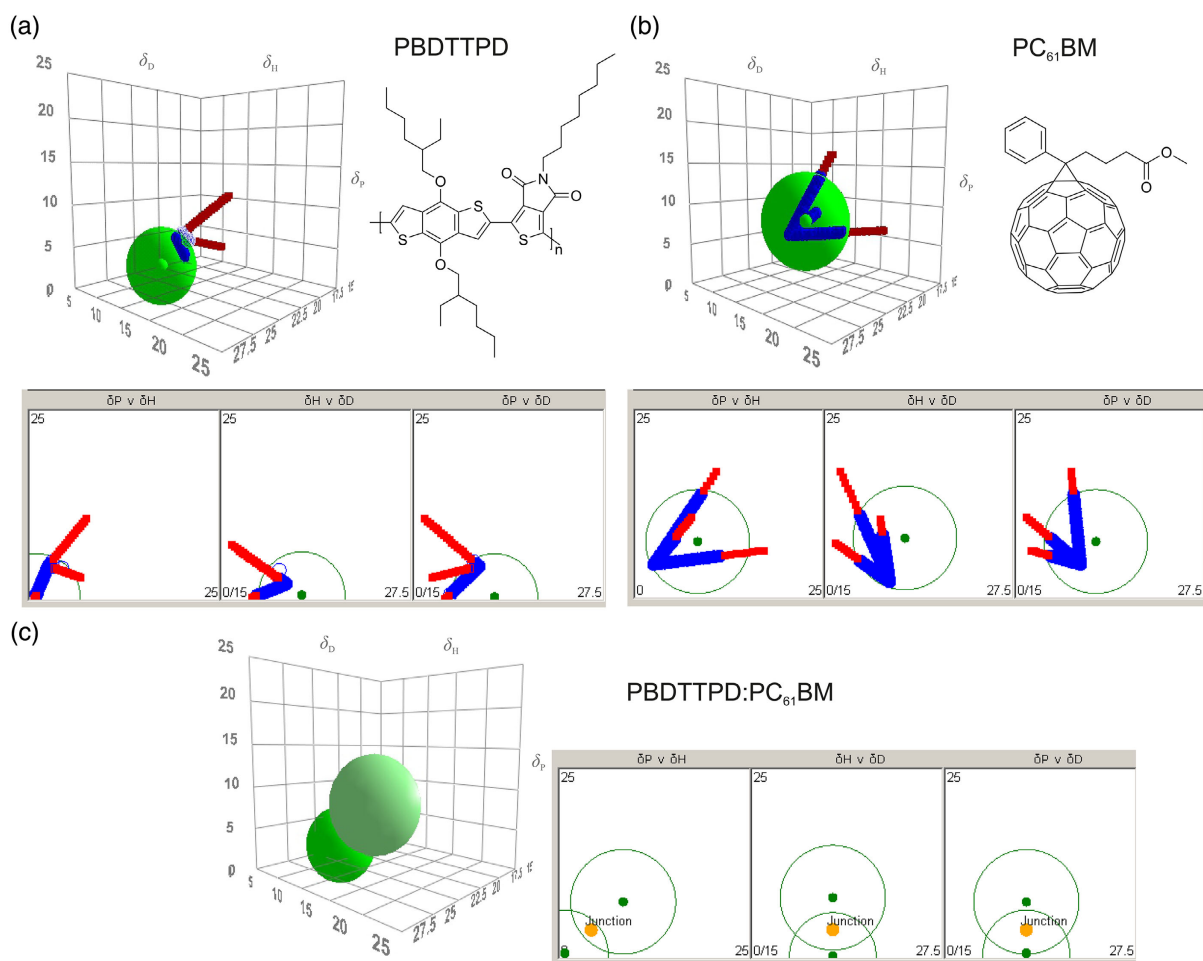
Figure 1. a) The polymer PBDTTPD and b) the fullerene $PC_{61}BM$, together with their chemical structures. c) Hansen spheres and intersection of the PBDTTPD and $PC_{61}BM$ spheres. HSPs of the chlorobenzene:cosolvent mixtures which are considered good (blue dots) or poor (red dots) for the dissolution of the specific solutes. From the spherical fit around the good solvent mixtures, the HSPs of the solutes are derived from the center coordinate of the sphere (green) and its radius R_0.

PBDTTPD batches that were less soluble in the reference solvent chlorobenzene, are discussed in the Supporting Information. To determine the HSPs of the semiconductor components, PBDTTPD and $PC_{61}BM$ were separately dissolved in mixtures of a good main solvent (here chlorobenzene) and a cosolvent. The latter was well miscible with the main solvent but poorly dissolved the respective semiconductors. We dissolved the polymer PBDTTPD in solvent mixtures of chlorobenzene and either of the cosolvents acetone, oleic acid, or cyclohexane at different chlorobenzene:cosolvent ratios. The cosolvents were chosen to mostly change either the hydrogen, the polar, or the dispersive HSP component. To determine the solubility limit, $1 \, mg \, mL^{-1}$ solutions of the polymer in each chlorobenzene:cosolvent binary mixture were prepared at room temperature, dissolved overnight and centrifuged afterward. The supernatant was separated from the precipitates and diluted to measure the remaining solid content in solution by UV–vis absorption spectrophotometry, upon which the solvent mixture is categorized into good or poor, using a solubility threshold of $0.5 \, mg \, mL^{-1}$. All results of good or poor solubility were introduced into the HSP software. The data fit

Table 1. HSP of the polymer PBDTTPD, the fullerene $PC_{61}BM$, and the mixture of PBDTTPD and $PC_{61}BM$.

Material	δ_D [MPa$^{1/2}$]	δ_P [MPa$^{1/2}$]	δ_H [MPa$^{1/2}$]	R_0 [MPa$^{1/2}$]
PBDTTPD	20.00	0.57	0.24	5.6
$PC_{61}BM$	20.00	7.24	7.78	6.8
PBDTTPD:$PC_{61}BM$	20.0	3.6	3.6	–

produced the solubility sphere of PBDTTPD in Hansen space, as shown in Figure 1a. The HSPs of PBDTTPD are also shown in **Table 1**. While the HSP coordinates of the polymers of different molecular weights were rather similar, the radius of the solubility sphere R_0 of PBDTTPD with $\overline{M_n} = 19 \, kg \, mol^{-1}$ was the largest. This is in accordance with the observation of a much higher solubility of this PBDTTPD fraction in the reference solvent chlorobenzene (see Figure S1–S3 and Table S1, S2, Supporting Information, for comparison), for which it was selected to continue our experiments.

The same procedure was applied to the fullerene $PC_{61}BM$ (Figure 1b) and $PC_{71}BM$ (Figure S1, S2, Table S1, Supporting Information), using 6 mg mL^{-1} solutions in binary chlorobenzene:cosolvent mixtures and a solubility threshold of 4 mg mL^{-1}. As cosolvents either acetone, isopropanol, or dimethylsulfoxide (DMSO) were used, similar to the earlier work by Machui et al.[35] The HSPs of $PC_{61}BM$ and $PC_{71}BM$ that we found, are in good agreement with the data that were previously reported in the literature.[35,36] As we found better solubility of $PC_{61}BM$ in chlorobenzene than of $PC_{71}BM$, and in light of the higher relevance for industrial fabrication due to its lower price, we continued our investigations using $PC_{61}BM$.

To this point, solutions of the individual semiconductors were investigated. The HSPs of semiconductor mixtures were then estimated as the center of the intersection of the two individual component spheres (Figure 1c). This intersection contains all solvent candidates that may be suitable to dissolve $PBDTTPD:PC_{61}BM$ blends. Starting from a database of 1239 halogenated and nonhalogenated solvents, a total of 14 solvents (i.e., hexachloroethane, phosphorus trichloride, hexamethyl benzene, isopropyl benzene (cumene), α-methylstyrene, bromotrichloro methane, trimethylbenzene, 1,2,3,5-tetramethylbenzene, 1,2,3,4-tetramethylbenzene, pentachloro ethane, toluene, mesitylene, chlorobenzene, and diphenylmethane) was found within the intersection. These 14 solvents were then ranked for their applicability in large-scale processing and their ecotoxicity, initially using the following gate criteria: 1) Relative evaporation rate (RER, relative to *n*-butyl acetate) >5 or boiling point (bp) <180 °C. 2) RER < 150. 3) Liquid at room temperature (20 °C); melting point (mp) <20 °C; bp >20 °C. 4) Nonhalogenated. 5) Solvents that are not classified as acute toxic (GHS06) or health hazardous (GHS08). 6) Price <1000 € L^{-1}.

Applying these gate criteria, however, only yielded one solvent candidate (α-methylstyrene) for the preparation of $PBDTTPD:PC_{61}BM$ solutions. Considering that the HSPs and the solubility spheres were determined at room temperature, and considering that the solubility of the polymer:fullerene blend increases toward higher solvent temperatures, we expanded the radius of the polymer and fullerene spheres R_0 to 10 MPa$^{1/2}$. Within the respective intersection, we then found 257 solvent candidates. Out of these solvent candidates, 134 were nonhalogenated, but only 15 fitted all gate criteria (Table S3, Supporting Information). As the solubility of the polymer in the reference solvent chlorobenzene was significantly lower than the solubility of $PC_{61}BM$, the solvents were prioritized according to their distance to PBDTTPD in the Hansen space.

The eight most suitable solvent candidates, i.e., α-methylstyrene, *p*-xylene, *o*-xylene, ethoxybenzene, dipentene (racemic limonene), eucalyptol (1,8-cineole), benzaldehyde (BA), and anisole, were tested for their thin-film-forming properties. Therefore, we dissolved PBDTTPD (8 mg mL^{-1}) and $PC_{61}BM$ (12 mg mL^{-1}) separately as well as blends of $PBDTTPD:PC_{61}BM$ (weight ratio 1:1.5, total concentration of 20 mg mL^{-1}) in the solvent candidates. Then we spin coated thin films of the neat semiconductors and their blends on glass substrates at elevated solution temperatures (60, 80, or 110 °C). The solvents dipentene, α-methylstyrene, eucalyptol, *o*-xylene, and *p*-xylene (**Figure 2**a) yielded good thin-film quality (color, homogeneity, no large particle formation), comparable with thin films deposited from

chlorobenzene. The solvents anisole, ethoxybenzene, and BA failed this test. The solvent candidate eucalyptol was a particularly unexpected outcome of the HSP study as it is none of the commonly investigated solvents for solar cell fabrication. Most importantly, eucalyptol is an all-ecofriendly solvent that complies with all other processing conditions that are necessary for large-area thin-film deposition.

2.2. Solar Cells with Light-Harvesting Layers Processed from One Solvent

After identifying the nonhalogenated solvent candidates by HSP analysis, we fabricated inverted solar cells comprising indium tin oxide (ITO), ZnO, $PBDTTPD:PC_{61}BM$, MoO_x, Ag (inset of Figure 2b). We deposited the light-harvesting layer from 85 °C warm solution which is compatible with future large-scale deposition on water-heated coating machines and hence is an important advancement over previous reports on PBDTTPD solar cells that utilized significantly higher (>100 °C[40,41]) deposition temperatures. The current density–voltage (*J–V*) curves of the solar cells are shown in Figure 2b, and their key parameters, i.e., short-circuit current density (J_{SC}), fill factor (FF), open-circuit voltage (V_{OC}), and PCE, are shown in **Table 2**. Reference solar cells cast from chlorobenzene achieved a maximum PCE of 4.4%, complying with previous reports on PBDTTPD solar cells (3.4–7.3%, $\overline{M_n}$ = 23–39 kg mol^{-1}, using $PC_{71}BM$[41]). The light-harvesting layers are very homogenous according to the atomic force micrographs in Figure 2c. The corresponding root-mean-square roughnesses R_q of this and all further layers are shown in Table 2. The absorbance spectrum of the light-harvesting layer processed from chlorobenzene in Figure 2d is very similar to previous reports with most pronounced contributions from PBDTTPD in the wavelength regime beyond 450 nm and $PC_{61}BM$ dominating the spectrum in the wavelength regime below 450 nm, with its characteristic feature at 330 nm.[42] Solar cells cast from the solvent candidate *o*-xylene exhibited equally good film forming properties and similar absorbance characteristics, yielding an almost identical average PCE of 4.2%, whereas all other solvents produced only moderate results.

2.2.1. α-Methylstyrene

With a PCE of 1.4%, the next best performance was achieved using α-methylstyrene. The *J–V* curves of the solar cells show a nonsaturating photocurrent under reverse bias and under illumination, which lets us conclude that the photogenerated charge carriers are extracted rather inefficiently. Figure 2c shows the topography of the $PBDTTPD:PC_{61}BM$ layers processed from α-methylstyrene. Similar to the absorber layers that were deposited from chlorobenzene or *o*-xylene, α-methylstyrene produces rather smooth and homogeneous light-harvesting layers ($R_q < 4$ nm) without any indication of phase separation of polymers or fullerenes.

One reason for the poor performance of α-methylstyrene-processed solar cells may be found in the absorbance of the layers (Figure 2d), which exhibits a reduced absorbance feature at 330 nm, and hence presumably altered electronic properties of $PC_{61}BM$. Interestingly, this effect showed to be heating time
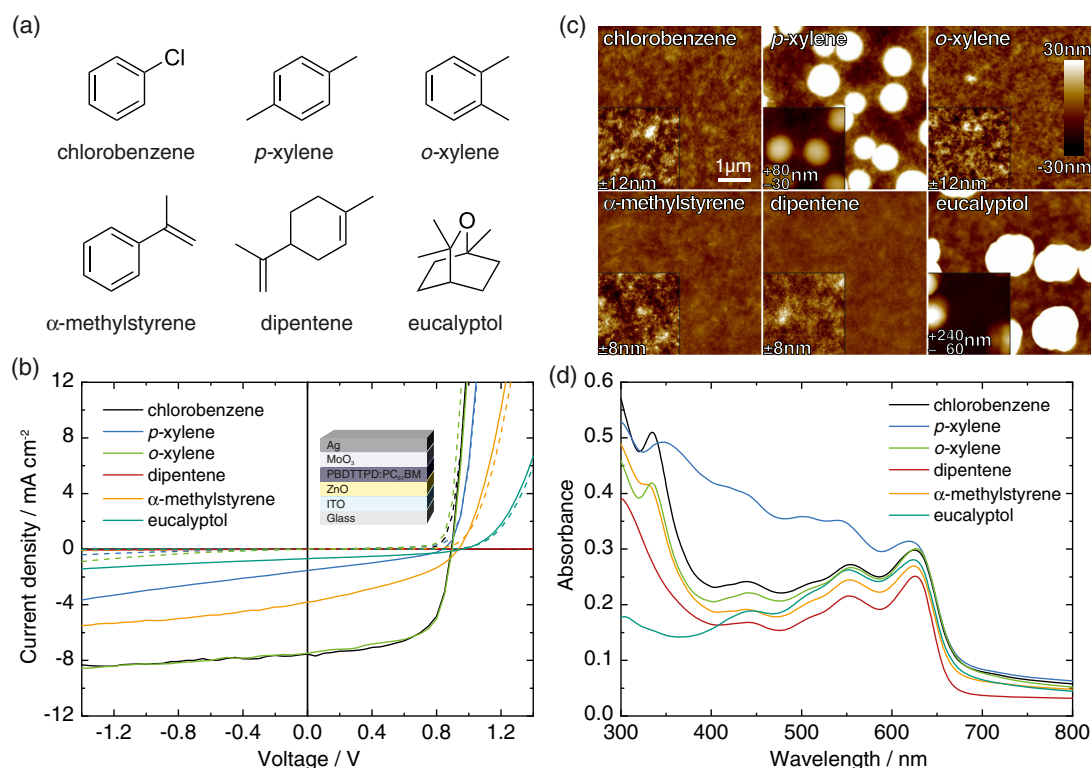
Figure 2. a) Chemical structures of the solvents considered in this study. b) Representative J–V curves of solar cells under illumination (solid lines) and in the dark (dashed lines) comprising PBDTTPD:PC$_{61}$BM light-harvesting layers, cast from different neat solvents. The inset shows the inverted ITO/ZnO/PBDTTPD:PC$_{61}$BM/MoO$_x$/Ag device architecture. c) AFM topography of PBDTTPD:PC$_{61}$BM layers deposited from different neat solvents using the same topography scale of ± 30 nm on all images to facilitate comparison (5×5 µm^2). All insets (2.5×2.5 µm^2) use different topography scales as denoted to better visualize the most important features. d) UV–vis absorbance of PBDTTPD:PC$_{61}$BM layers deposited from different neat solvents.

Table 2. Key parameters of PBDTTPD:PC$_{61}$BM solar cells that were deposited from different neat solvents, averaged over at least four individual devices, as well as the surface roughness R_q of the AFM topography in Figure 2.

Solvent	J_{SC} [mA cm^{-2}]	FF [%]	V_{OC} [V]	PCE [%][a]	R_q [nm]
Chlorobenzene	7.6	61	0.89	4.2 (4.4)	3.5
p-Xylene	1.5	31	0.84	0.4 (0.4)	21.4
o-Xylene	7.4	63	0.89	4.2 (4.4)	3.6
Dipentene	0.0	–	–	0	1.8
α-Methylstyrene	3.9	37	0.94	1.4 (1.4)	2.4
Eucalyptol	0.6	38	0.96	0.2	66.7

[a]Maximum PCE in parentheses.

dependent (Figure S4c, Supporting Information): while the PC$_{61}$BM absorbance feature prevailed for about 30 min upon contact with α-methylstyrene at room temperature, after 2 days of solvent contact (85 °C), the characteristic 330 nm absorbance peak was substantially reduced. Notably, the dissolution of PBDTTPD requires rather hours than minutes, so that the PC$_{61}$BM decay is inherent. In addition, changes in the absorption spectra of the solvent indicated polymerization of the α-methylstyrene itself (Figure S4d, Supporting Information), and the corresponding layers were very inhomogeneous.

2.2.2. Dipentene

Although enantiomers of dipentene (limonene) had been successfully used in the past to deposit certain polymer layers of organic light-emitting diodes and field effect transistors,[43] in the context of OSCs only the deposition of polymer:fullerene layers or polymer/fullerene bilayers had been shown, yet without reporting device performance.[44,45] In our experiments, solar cells cast from dipentene showed essentially no photovoltaic performance at all. No distinct diode characteristics with significant device currents in forward direction were observed. We attribute the poor performance of solar cells processed from dipentene to chemical fullerene degradation: While the absorption spectrum in the long-wavelength polymer regime of Figure 2d does not differ much from the chlorobenzene-processed reference, the 330 nm fullerene feature in the dipentene-cast layer is fully missing. We observed the disappearance of the PC$_{61}$BM absorbance feature already in the dipentene solution (Figure S4a, Supporting Information), which lets us suspect a chemical reaction between PC$_{61}$BM and dipentene possibly facilitated at elevated temperatures. The chemical functionalization of PC$_{61}$BM by the solvent and thereby its partial degradation of the π-conjugation may

**ADVANCED
SCIENCE NEWS**

www.advancedsciencenews.com

**ADVANCED
ENERGY & SUSTAINABILITY
RESEARCH**
Open Access

www.advenergysustres.com

severely hamper charge carrier transport, leading to rather insulating properties of the layer.

2.2.3. p-Xylene and Eucalyptol

Depositing PBDTTPD:PC$_{61}$BM from either p-xylene or eucalyptol produced solar cells with PCEs below 1%, which is partly caused by a FF below 40%. The J–V curves of the solar cells show a nonsaturating photocurrent under reverse bias, which lets us conclude that the photogenerated charge carriers are extracted rather inefficiently.

As shown in Figure 2c, the deposition of the light-harvesting layers from p-xylene or eucalyptol produced distinct lens-shaped features of several tens of nanometers in height and an overall $R_q > 20$ nm. Such features are often observed in polymer: PC$_{61}$BM (or polymer:PC$_{71}$BM) layers and correspond to phase separated regions of high fullerene content.[46–48] As a consequence, the remaining layer must be severely depleted of acceptors, which determines the shape of the J–V curve and inhibits proper solar cell performances.[49]

In the layers cast from eucalyptol, the absorbance in the PC$_{61}$BM region (around 330 nm) was significantly reduced as compared with the reference absorbance spectrum of layers processed from chlorobenzene. Although we found PC$_{61}$BM clusters (average diameter 1.3 μm, height >200 nm) with supposedly high absorption at 330 nm, the overall absorption is vastly dominated by the much larger PC$_{61}$BM-depleted areas which are more transparent in this spectral regime. For the layers cast from p-xylene, we made a subtly different observation: even though we identified fullerene clusters, the overall absorbance in the spectral region below 500 nm was enhanced. We attribute this to significant diffuse scattering of light at the fullerene clusters (average diameter 0.8 μm, height 70 nm). The absorption of the layer from p-xylene, as determined from measuring transmission and reflection in an integrating sphere, was much more similar to homogeneous layers without fullerene clusters (Figure S5, Supporting Information). Thus, the absorbance of the layers from eucalyptol and p-xylene are influenced by their surface topography and together both explain the low performance of the corresponding solar cells.

2.2.4. Choice of Solvents

Not all solvents identified by the HSP approach were suitable for device fabrication. Dipentene and α-methylstyrene exhibited chemical reactivity with PC$_{61}$BM, prohibiting efficient photovoltaic performance, although they produced homogenous light-harvesting layers on the nanoscale with no obvious phase separation. Even though chemical compatibility may still be provided at low temperatures and during short contact times, we discarded dipentene and α-methylstyrene, as experimental reproducibility could hardly be guaranteed. Solar cells cast from p-xylene or eucalyptol did also not reach to the photovoltaic efficiency of the chlorobenzene reference, due to severe polymer: fullerene phase separation, which may be a consequence of liquid–liquid phase separation and fullerene clustering during solvent evaporation.[50] Interestingly, in the polymer:fullerene thin-film formation, p-xylene differed drastically from o-xylene,

where no fullerene aggregates were observed and thus high performance was achieved. We attribute this observation to some differences in their physicochemical properties (molar volume, density, boiling point, see Table S3, Supporting Information) and the higher solubility of PC$_{61}$BM in o-xylene[51] that may prevent demixing during solvent evaporation.

However, moderate solar cell performances due to fullerene aggregation are a known problem, with the use of cosolvents or solvent additives being a viable mitigation measure to suppress phase separation and manipulate the nanomorphology, thus optimizing the device performance. This is why we took on o-xylene, p-xylene, and eucalyptol as main solvents for further studies on solvent mixtures in the following sections.

2.3. Solar Cells with Light-Harvesting Layers Processed from Solvent/Additive Combinations

While the HSP analysis produces the most suitable solvents for the dissolution of the two semiconductors, the bulk heterojunction formation in these solvents may not be optimal due to different interactions with the semiconductors and hence some distinct phase separation as observed in the experiments described earlier. In this case, the ultimate film solidification can be controlled by solvent additives to enhance the bulk heterojunction formation. The most common solvent additives are high-boiling-point solvents in which the solutes or components thereof exhibit different solubilities. They are added in small amounts to the main solvent before casting thin films. As a consequence of the low initial volume fraction of additives, they hardly influence the solute's total solubility in the initial solution, but they gain importance toward the later stages of drying when the main solvent has mostly evaporated. This is why they are difficult to describe with the HSP approach. Derivatives of halogenated alkanes,[52] alkane dithiols,[53] and naphthalenes[54] are the most commonly used additives for the deposition of organic bulk heterojunctions.

In Section 2.2, we identified p-xylene and eucalyptol as potentially suitable solvents for the deposition of PBDTTPD:PC$_{61}$BM layers. Yet, strong phase separation occurs during drying. p-Xylene has only rarely been used in earlier studies.[55–57] So far, eucalyptol has not been reported as solvent for the deposition of bulk heterojunctions at all. To enhance the performance of the solar cells deposited from p-xylene or eucalyptol, we tested the solvent additives 1-chloronaphthalene (CN), which had previously been reported to improve the device performance of PBDTTPD:PC$_{71}$BM solar cells,[41] and p-anisaldehyde (AA), which was reported as an ecofriendly alternative to the omnipresent 1,8-diiodooctane in a variety of polymer:fullerene solar cells.[58] For reference, again, we fabricated solar cells comprising light-harvesting layers deposited from chlorobenzene, chlorobenzene+CN (addition of 5% by volume), and chlorobenzene+AA (2%). **Figure 3**a shows representative J–V curves of the corresponding solar cells and the reference solar cell. Their key parameters are shown in **Table 3**.

In accordance with earlier reports, the addition of CN or AA to chlorobenzene solutions improved the PCE of our PBDTTPD: PC$_{61}$BM solar cells from 4.2% to 4.6% or 4.4%, respectively.

When the additives CN or AA were used for the deposition of light-harvesting layers from p-xylene solutions (Figure 3b), we
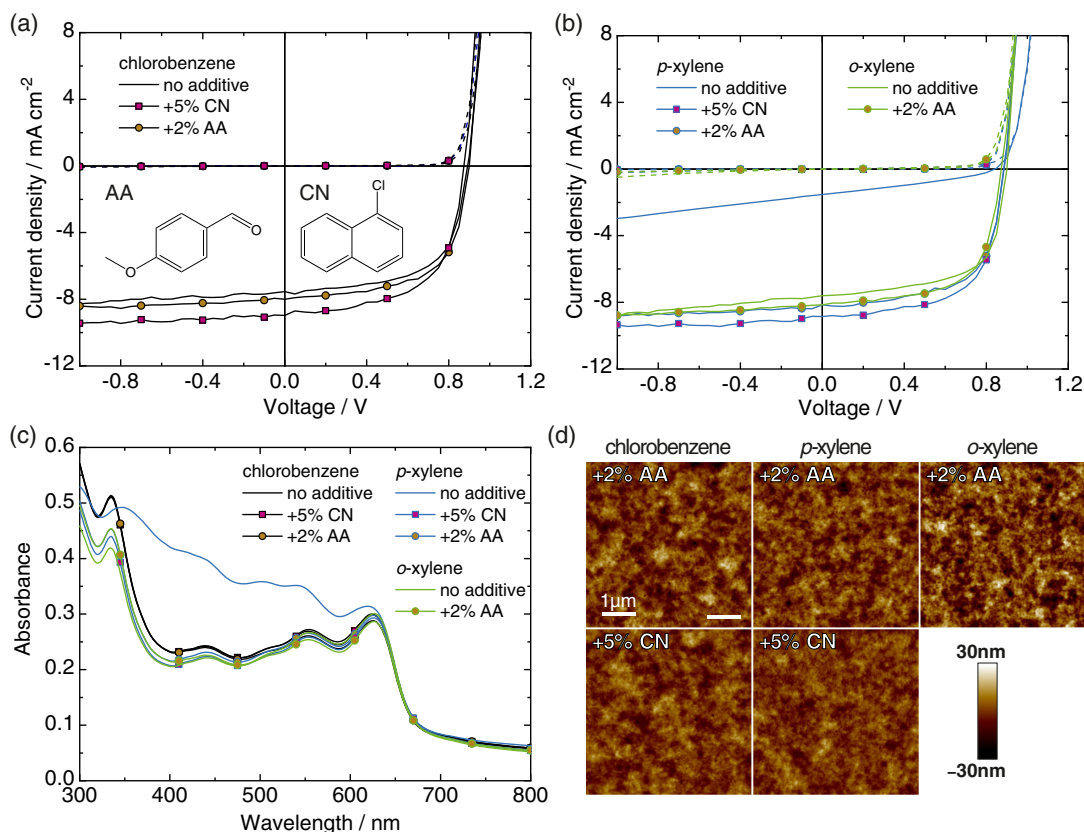
ADVANCED
SCIENCE NEWS
www.advancedsciencenews.com

ADVANCED
ENERGY & SUSTAINABILITY
RESEARCH
Open Access
www.advenergysustres.com

Figure 3. a) Representative J–V curves of solar cells with light-harvesting layers of PBDTTPD:PC$_{61}$BM cast from chlorobenzene plus either of the solvent additives AA (2%) or CN (5%). Inset: chemical structures of AA and CN. b) J–V curves of solar cells cast from p-xylene or o-xylene using solvent additives. c) UV–vis absorbance of the respective PBDTTPD:PC$_{61}$BM layers. d) AFM topography of the layers (5×5 μm^2).

Table 3. Key parameters of PBDTTPD:PC$_{61}$BM solar cells that were deposited from different solvent/additive combinations, averaged over at least four individual devices, as well as the surface roughnesses R_q of the AFM topography in Figure 3. For reference, data from using neat solvents are reproduced from Table 2.

Solvent	Solvent additive	J_{SC} [mA cm^{-2}]	FF [%]	V_{OC} [V]	PCE [%][a]	R_q [nm]
Chlorobenzene	–	7.6	61	0.89	4.2 (4.4)	3.5
	5% CN	8.8	60	0.87	4.6 (4.8)	5.2
	2% AA	7.8	63	0.90	4.4 (4.5)	6.2
p-Xylene	–	1.5	31	0.84	0.4 (0.4)	21.4
	5% CN	8.9	61	0.88	4.8 (5.0)	4.6
	2% AA	8.3	63	0.89	4.7 (4.8)	5.8
o-Xylene	–	7.4	63	0.89	4.2 (4.4)	3.6
	2% AA	8.3	63	0.87	4.6 (4.9)	7.7
Eucalyptol	–	0.6	38	0.96	0.2	66.7
	5% CN	4.9	36	0.98	1.7	4.0
	2% AA	3.3	31	0.99	1.0	4.2

[a]Maximum PCE in parentheses.

found a drastic increase in the device performance. Solar cells from p-xylene+CN or p-xylene+AA exhibited PCEs of 4.8% or 4.7%, respectively, which was far better than the PCE of 0.4% upon layer deposition from neat p-xylene. This result also matched the PCE = 4.6% of solar cells fabricated from the more often used o-xylene in combination with AA.

Figure 3c,d shows the absorbance of the light-harvesting layers deposited from the various solvent/additive combinations and their surface topography recorded by atomic force microscopy (AFM). The absorbance of the PBDTTPD:PC$_{61}$BM layers that were deposited from chlorobenzene+CN or chlorobenzene+AA almost matched the absorbance of the layers that were processed from neat chlorobenzene. At the same time, we observed only a slight increase in the surface roughness which may hint at some minor phase separation induced by polymer aggregation. The absorbance of layers that were deposited from p-xylene+CN, p-xylene+AA, o-xylene, or o-xylene+AA was identical, but distinctly different from the layers deposited from neat p-xylene. In contrast to the deposition from neat p-xylene, upon which the absorbance of the layer was strongly affected by scattering, using either additive produced smooth layers with no aggregates. Thus no scattering was observed, and hence the corresponding absorbance of the layers resembled

**ADVANCED
SCIENCE NEWS**

www.advancedsciencenews.com

**ADVANCED
ENERGY & SUSTAINABILITY
RESEARCH**
Open Access

www.advenergysustres.com

the absorbance of layers deposited from chlorobenzene. Notably, while adding AA to *p*-xylene solutions prevented microscopic phase separation by demixing, supposedly through nanoscopic polymer aggregation,[59] and led to a huge PCE enhancement from 0.4% to 4.7%, it only slightly improved the solar cell performance with PBDTTPD:PC$_{61}$BM layers deposited from *o*-xylene.

Also in layers deposited from eucalyptol, severe phase separation was found to be one reason for the low device performance. Again, CN or AA improved the layer formation with no fullerene aggregates being present on the nanoscale. However, the overall lower solubility of the fullerene in eucalyptol led to inhomogeneous layers, even when using solvent additives (AFM topography in Figure S6b, photos in Figure S6c, Supporting Information). As a consequence, the PCEs consolidated below 2% (Table 3, J–V curves in Figure S6a, Supporting Information).

2.4. Solar Cells with Light-Harvesting Layers Deposited from Binary Solvents

One of the ideas behind the HSP approach is the tailoring of specific solvent properties by combination of two neat solvents (binary mixture). For example, earlier reports mimicked the HSPs of *o*-dichlorobenzene by mixing mesitylene with acetophenone.[60] However, the mesitylene/acetophenone (27:73 by volume) mixture with the HSP closest to *o*-dichlorobenzene did not produce the best-performing polythiophene:PC$_{61}$BM solar cells, but the 80:20 mixture with far less acetophenone. Similarly, *p*-xylene/acetophenone and *p*-xylene/BA were used as binary solvents, with BA exhibiting a boiling point and viscosity similar to *o*-dichlorobenzene.[61] A mixture of carbon disulfide and acetone was used to replace CB for the fabrication of solar cells.[62]

In this study, having determined the HSPs of PBDTTPD:PC$_{61}$BM before, we have the opportunity to choose the solvent mixture that best matches the HSPs of this blend rather than mimicking a (randomly chosen) solvent such as *o*-dichlorobenzene. From our HSP study, we concluded that a 1:1 mixture of *p*-xylene and BA, which is close to the junction of the PBDTTPD and PC$_{61}$BM Hansen spheres, is a good candidate to dissolve PBDTTPD:PC$_{61}$BM. The combination of *p*-xylene and BA appears particularly interesting as *p*-xylene is a good solvent for PBDTTPD (and other polymers), whereas BA was reported to dissolve fullerenes.[36] Thus, we prepared *p*-xylene:BA and, for comparison, *o*-xylene:BA solutions. We found that PBDTTPD is poorly soluble in a 1:1 mixture of *p*-xylene:BA and PBDTTPD precipitates occurred. In addition, in solutions and layers spin cast from *p*-xylene:BA hardly any polymer-specific blue color was visible (Figure S7, Supporting Information). This may originate from the large BA fraction in the solvent mixture which strongly reduces the PBDTTPD solubility. In addition, due to the lower boiling point of *p*-xylene (138 °C) versus BA (179 °C), we speculate that, in the final stage of drying, a significant fraction of *p*-xylene has evaporated, shifting the solvent ratio *p*-xylene:BA from 1:1 to a BA-dominated drying process. If this speculation is true, layer formation should be improved by increasing the amount of *p*-xylene in the initial solution, as should the solubility of PBDTTPD. Indeed, lowering the BA volume fraction to 20%, 10%, 5%, or 2%

significantly enhanced the layer quality (Figure S7, Supporting Information). We thus disregarded the 1:1 mixture close to the HSP of the PBDTTPD:PC$_{61}$BM blend and fabricated solar cells from the *o*-xylene:BA and *p*-xylene:BA mixtures with lower BA content. Representative J–V curves are shown in **Figure 4**a, and the corresponding key parameters are shown in **Table 4**. For BA fractions of 5%, we found optimal solar cell performance. For higher BA volume fractions (10%), the device performance was
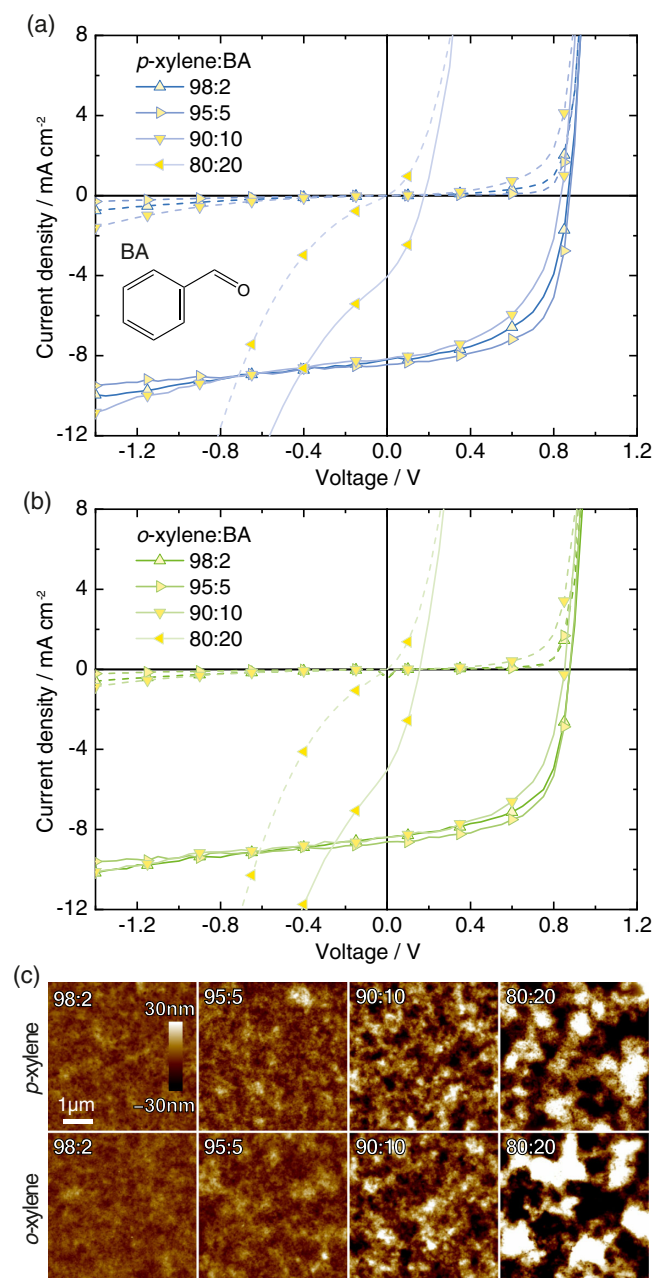

Figure 4. a) Representative J–V curves of solar cells comprising PBDTTPD:PC$_{61}$BM light-harvesting layers cast from *p*-xylene:BA. Inset: chemical structure of BA. b) J–V curves of solar cells cast from *o*-xylene:BA. c) AFM topography of the photoactive layers (5 × 5 μm^2), using the same topography scale of ±30 nm for all images.

ADVANCED
SCIENCE NEWS

www.advancedsciencenews.com

ADVANCED
ENERGY & SUSTAINABILITY
RESEARCH
Open Access

www.advenergysustres.com

Table 4. Key parameters of PBDTTPD:PC$_{61}$BM solar cells that were deposited from different solvent/BA combinations, averaged over at least four individual devices, as well as the surface roughnesses R_q of the AFM topography in Figure 4 and 5.

Solvent	Solvent:BA ratio	J_{SC} [mA cm^{-2}]	FF [%]	V_{OC} [V]	PCE [%][a]	R_q [nm]
p-Xylene	98:2	7.9	57	0.87	3.9 (4.2)	3.7
	95:5	8.2	63	0.87	4.5 (4.7)	6.0
	90:10	8.4	53	0.84	3.7 (3.8)	11.4
	80:20	3.9	31	0.16	0.2 (0.4)	19.3
o-Xylene	98:2	8.3	61	0.87	4.5 (4.6)	3.6
	95:5	8.5	62	0.87	4.5 (4.8)	5.8
	90:10	8.3	56	0.85	4.0 (4.1)	11.4
	80:20	5.4	30	0.12	0.2 (0.3)	32.2
Eucalyptol	90:10	0.7	31	0.63	0.2 (0.2)	27.4
	90:10 + 2% AA	5.9	43	0.95	2.4 (3.0)	5.3

[a]Maximum PCE in parentheses.

diminished by shunting, as became visible in the gradually increasing current under reverse bias both under illumination and in the dark. This was most drastically visible when the devices were fabricated from 80:20 mixtures of p-xylene:BA, where all key parameters, including the V_{OC}, were significantly deteriorated, yielding PCEs of less than 1%. This deterioration was accompanied by a roughening of the surface with increasing BA content, eventually leading to a large peak-to-valley roughness and hence increased chances of pinhole formation in the polymer:fullerene layer which accounts for shunting. Toward lower volume fractions of BA of 5% or 2%, the surface became smoother. The optimum performance of the solar cells was achieved when using 5% of BA and 95% of p-xylene. Similarly, volume fractions of 5% and 2% of BA in o-xylene-based solutions yielded best device performances. In both cases, the cosolvent BA rather played the role of a solvent additive as described earlier in Section 2.3. Interestingly, the binary solvent approach led to the same conclusion on the use of solvent/additive mixtures as drawn earlier. When using p-xylene, a certain amount of second solvent seems to be necessary to suppress liquid–liquid demixing and to optimize the morphology on the nanoscale. For o-xylene, no detrimental phase separation occurs upon deposition from the neat solvent, which is why the cosolvent BA investigated herein hardly changed the morphology. Again, we conclude that the cosolvent BA is responsible for the formation of the layer morphology and hence the final device performance rather than the different properties of p-xylene and o-xylene.

2.5. Eucalyptol

Among the solvents that were identified by the HSP study, eucalyptol stands out being ecofriendly, biodegradable, nontoxic, and a natural constituent of the essential oil fraction of several plants.[63] It would therefore be the ideal solvent to be part of a fully sustainable fabrication process of OSCs. Yet, as discussed earlier, eucalyptol alone does not produce efficient light-harvesting layers which may partly be due to the poor solubility

of PC$_{61}$BM and PC$_{71}$BM in eucalyptol and hence the formation of fullerene aggregates. As BA is known for its high fullerene solubility,[36] we deposited layers of PBDTTPD:PC$_{61}$BM from mixtures of eucalyptol and BA both of which have about similar boiling points (177 and 179 °C). Notably, BA is also biodegradable, can be gained from several essential oils and is even used in cosmetics,[64] rendering it the perfect ecofriendly and sustainable cosolvent to eucalyptol. Again, we observed that a high volume fraction of BA (50%) hampers polymer dissolution, and hence a yellowish PC$_{61}$BM texture dominates the layer absorption (Figure S7, Supporting Information). Reducing the amount of BA in the binary solvent (80:20, 90:10) improved the layer quality and produced appropriate spectral absorption (color), however, with some smaller homogeneously distributed fullerene clusters still being present in the layer (**Figure 5**b) and with the corresponding solar cells yielding only PCEs of 0.2%. This is why we set out to use an additional solvent additive, here the ecofriendly AA, which further suppresses the formation of fullerene clusters. Figure 5a shows J–V curves comparing representative devices with PBDTTPD:PC$_{61}$BM cast from eucalyptol:BA (90:10) mixtures with and without 2% of AA added. The corresponding key parameters are shown in Table 4. Upon the addition of AA, no fullerene clusters are visible, the BHJ surface appears more homogeneous and the device PCE improved significantly to average 2.4%, with a maximum PCE of 3.0%. At this stage, the reason for the lower PCE is beyond the scope of this work. However, although the OSC performance is still somewhat below the devices fabricated from xylenes, the combination of
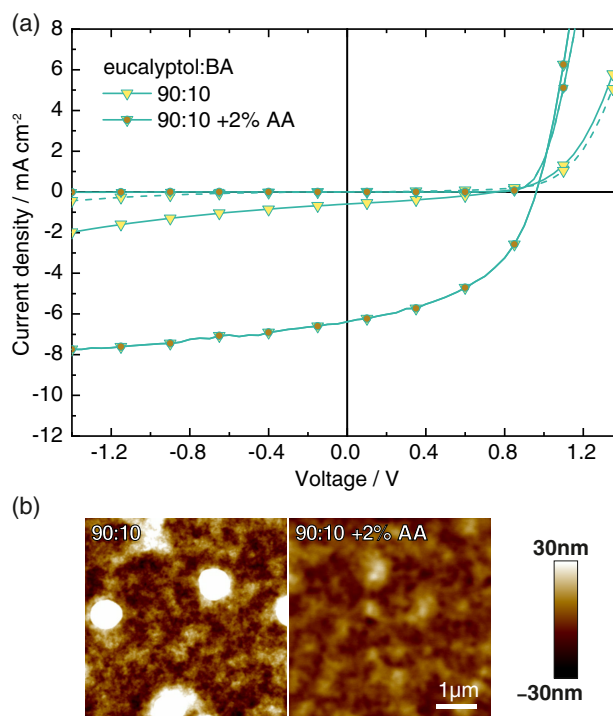

Figure 5. a) Representative J–V curves of PBDTTPD:PC$_{61}$BM solar cells with light-harvesting layers cast from eucalyptol:BA (90:10) using the solvent additive AA. b) AFM topography of the corresponding PBDTTPD:PC$_{61}$BM layers (5 × 5 μm^2).

eucalyptol, BA, and AA may become interesting for a future eco-friendly fabrication of OSC, reducing regulatory production constraints and spreading a pleasant odor.

3. Conclusion

The formation of light-harvesting polymer:fullerene blends advances in three steps: 1) dissolution of the bulk-heterojunction components, 2) deposition of the wet film and drying, and 3) thin-film solidification. The HSP approach is a powerful tool to facilitate the first step of layer formation, i.e., the dissolution of the organic semiconductors. The second step is mostly ruled by the boiling points of the solvents. Here, we identified the eight nonhalogenated solvents α-methylstyrene, *p*-xylene, *o*-xylene, ethoxybenzene, dipentene, eucalyptol, BA, and anisole with a potentially lower environmental impact, good wetting of sample surfaces, and reasonable boiling points as good solvents to a PBDTTPD:$PC_{61}BM$ solute. However, the HSP analysis does not provide a reliable rationale to the third step, the layer formation, as solubility, miscibility, and kinetics during drying control the development of the BHJ morphology. This is why we had to discard all good (neat) solvents but *o*-xylene. Yet, using solvent additives such as AA or CN to control the second and third stages of layer drying broadens the choice of main solvents. The situation becomes even more complex, if a binary solvent is used, where the initially optimal solvent ratio gained from the HSP analysis may change during stage two, which is the initial drying process, e.g., due to different boiling points of the binary solvent components. In this case, the higher-boiling point solvent may rather act as a solvent additive as we exemplified by mixtures of *p*-xylene and BA. Other limitations to the HSP approach can be chemical reactions of the solvents with the solute as we have observed for α-methylstyrene and dipentene. The investigations presented in this work clearly demonstrate some of the limitations of the HSP formalism that are important to consider when looking for other suitable solvents for the deposition of bulk heterojunction solar cells. Yet, we found the solvent eucalyptol in our HSP study which is, as a natural product, fully ecofriendly and biodegradable, and which, in combination with the ecofriendly BA and AA produced OSC with good performance.

In addition, our study underlines the urgent need for high-performance polymers with a better solubility in "green" solvents to facilitate industrial uptake of OSC fabrication processes.

4. Experimental Section

HSPs and Choice of Solvents: Three different batches of PBDTTPD were synthesized according to literature procedures,[41,65] and the $\overline{M_n}$ of 15, 19, and 28 kg mol^{-1}, the average molecular weight per weight ($\overline{M_w}$) and the polydispersity index (Đ) of the polymers were estimated by gel permeation chromatography (GPC) on a PL-GPC220 instrument from Agilent Technologies based on monodispersed polystyrene standards at high temperature (150 °C) and utilizing *o*-dichlorobenzene as eluent. Solutions of the polymer (1 mg mL^{-1}) in chlorobenzene:cosolvent mixtures were prepared and dissolved overnight at 110 °C, cooled down to room temperature and centrifuged. The supernatant was removed and diluted for UV-vis absorption spectrometry (Shimadzu UV-2450) and compared with a calibration curve to measure the concentration of the diluted solutions and to determine the semiconductor's initial solubility before dilution. Good or

poor solvent mixtures were categorized based on the polymer's solubility being above or below a threshold of 0.5 mg mL^{-1}. Solutions of the fullerenes $PC_{61}BM$ and $PC_{71}BM$ (Nano-C, Inc.) in binary solvent mixtures (6 mg mL^{-1}) were prepared and the solubility threshold was set to 4 mg mL^{-1}. Similar to the aforementioned solutions, concentrated solutions of the semiconductors in chlorobenzene were prepared and centrifuged at room temperature to determine their maximum solubility. For all solvent mixtures and semiconductors, the result of good or poor solubilization was introduced into the software (HSPiP 4.1.04), and the data were fitted with a sphere to determine the HSP of the solute. The nonhalogenated solvents from within this sphere were used to prepare polymer (8 mg mL^{-1}), fullerene (12 mg mL^{-1}), and blend solutions (polymer concentration c_{pol} = 8 mg/mL, polymer:fullerene 1:1.5 w/w) to determine the general suitability for thin-film deposition by spin coating (1500 rpm, 30 s) of warm solutions (>60 °C) on precleaned soda lime glass substrates (2.5 × 2.5 cm^2). All solvents (Sigma Aldrich) were used as received.

Solar Cell Fabrication and Characterization: OSCs were fabricated according to the device architecture shown in the inset of Figure 2b. Patterned indium tin oxide (ITO, $R_{\square} \approx 13 \, \Omega$)-coated glass substrates were cleaned by sequential ultrasonication in acetone and isopropanol (10 min). Then the substrates were transferred into a nitrogen glovebox for the fabrication and characterization process. A ZnO electron extraction layer was spin cast from nanoparticle dispersion (Nanograde Ltd., 1 wt% in isopropanol, 4000 rpm, 30 s) and thermally annealed on a hotplate (80 °C, 10 min). The polymer PBDTTPD and $PC_{61}BM$ (Solenne, 99%) were dissolved (1:1.5 w/w, c_{pol} = 8 mg/mL) in the main solvent or solvent mixtures. Solvent additives were then added to the stock solution. Solvent mixtures of 2% and 5% were prepared by adding 2% or 5% (by volume) of the second solvent to the stock solution. All solvents (Sigma Aldrich) were used as received. The nonfiltered warm solutions (85 °C) were spun onto the samples (1000 rpm, 60 s) to form light-harvesting layers of 80–100 nm thickness. The as-cast devices were then transferred into a vacuum chamber (base pressure 10^{-6} mbar) to deposit MoO_3 (10 nm) and the Ag top electrode (100 nm) by thermal evaporation, using a shadow mask defining the photoactive area of the solar cell (3 × 3.5 mm^2).

Current density–voltage (*J–V*) curves were measured with a source-measurement unit (Keithley 238) under illumination from a spectrally monitored solar simulator (Oriel 300 W, 1000 W m^{-2}, ASTM AM 1.5 G), calibrated by a KG5 filtered silicon reference cell (91150-KG5, Newport). Layer thicknesses were measured with a tactile stylus profiler (Dektak XT, Bruker). Absorbance spectra were recorded using a UV–vis–near infrared (NIR) spectrophotometer (Cary 5000, Agilent Technologies) in two-beam transmission mode. The respective light-harvesting layers on glass substrates were prepared following the procedure described earlier. The topography was analyzed on an atomic force microscopy in tapping mode (Dimension ICON, Bruker, TESP tip) on solar cells next to the top electrodes.

Supporting Information

Supporting Information is available from the Wiley Online Library or from the author.

Conflict of Interest

The authors declare no conflict of interest.

Data Availability Statement

The data that support the findings of this study are available from the corresponding author upon reasonable request.

Keywords

green solvents, Hansen solubility parameters, nonhalogenated solvents, organic solar cells, solvent additives

[1] F. Machui, M. Hösel, N. Li, G. D. Spyropoulos, T. Ameri, R. R. Søndergaard, M. Jørgensen, A. Scheel, D. Gaiser, K. Kreul, D. Lenssen, M. Legros, N. Lemaitre, M. Vilkman, M. Välimäki, S. Nordman, C. J. Brabec, F. C. Krebs, *Energy Environ. Sci.* **2014**, *7*, 2792.

[2] F. C. Krebs, N. Espinosa, M. Hösel, R. R. Søndergaard, M. Jørgensen, *Adv. Mater.* **2014**, *26*, 29.

[3] D. Hengevoss, C. Baumgartner, G. Nisato, C. Hugi, *Sol. Energy* **2016**, *137*, 317.

[4] J. Zhao, Y. Li, G. Yang, K. Jiang, H. Lin, H. Ade, W. Ma, H. Yan, *Nat. Energy* **2016**, *1*, 15027.

[5] S. Rasool, Q. V. Hoang, D. Van Vu, T. T. Trang Bui, S.-M. Jin, T. T. Ho, C. E. Song, H. K. Lee, S. K. Lee, J.-C. Lee, S.-J. Moon, E. Lee, W. S. Shin, *J. Mater. Chem. A* **2019**, *7*, 24992.

[6] Y. Lin, Y. Firdaus, M. I. Nugraha, F. Liu, S. Karuthedath, A. Emwas, W. Zhang, A. Seitkhan, M. Neophytou, H. Faber, E. Yengel, I. McCulloch, L. Tsetseris, F. Laquai, T. D. Anthopoulos, *Adv. Sci.* **2020**, *7*, 1903419.

[7] Q. Liu, Y. Jiang, K. Jin, J. Qin, J. Xu, W. Li, J. Xiong, J. Liu, Z. Xiao, K. Sun, S. Yang, X. Zhang, L. Ding, *Sci. Bull.* **2020**, *65*, 272.

[8] R. Garcia-Valverde, J. A. Villarejo, M. Hösel, M. V. Madsen, R. R. Søndergaard, M. Jørgensen, F. C. Krebs, *Sol. Energy Mater. Sol. Cells* **2016**, *144*, 48.

[9] D. Landerer, D. Bahro, H. Röhm, M. Koppitz, A. Mertens, F. Manger, F. Denk, M. Heidinger, T. Windmann, A. Colsmann, *Energy Technol.* **2017**, *5*, 1936.

[10] Y. Huang, C. K. Luscombe, *Chem. Rec.* **2019**, *19*, 1039.

[11] D. Zimmermann, C. Sprau, J. Schröder, V. G. Gregoriou, A. Avgeropoulos, C. L. Chochos, A. Colsmann, S. Janietz, H. Krüger, *J. Polym. Sci., Part A: Polym. Chem.* **2018**, *56*, 1457.

[12] C. Capello, U. Fischer, K. Hungerbühler, *Green Chem.* **2007**, *9*, 927.

[13] R. K. Henderson, C. Jiménez-González, D. J. C. Constable, S. R. Alston, G. G. A. Inglis, G. Fisher, J. Sherwood, S. P. Binks, A. D. Curzons, *Green Chem.* **2011**, *13*, 854.

[14] W. Zhao, L. Ye, S. Zhang, M. Sun, J. Hou, *J. Mater. Chem. A* **2015**, *3*, 12723.

[15] F. Liu, Z. Zhou, C. Zhang, T. Vergote, H. Fan, F. Liu, X. Zhu, *J. Am. Chem. Soc.* **2016**, *138*, 15523.

[16] M. E. Farahat, C.-S. Tsao, Y.-C. Huang, S. H. Chang, W. Budiawan, C.-G. Wu, C.-W. Chu, *J. Mater. Chem. A* **2016**, *4*, 7341.

[17] L. Ye, Y. Xiong, H. Yao, A. Gadisa, H. Zhang, S. Li, M. Ghasemi, N. Balar, A. Hunt, B. T. O'Connor, J. Hou, H. Ade, *Chem. Mater.* **2016**, *28*, 7451.

[18] A. Wadsworth, R. S. Ashraf, M. Abdelsamie, S. Pont, M. Little, M. Moser, Z. Hamid, M. Neophytou, W. Zhang, A. Amassian, J. R. Durrant, D. Baran, I. McCulloch, *ACS Energy Lett.* **2017**, 1494.

[19] J. E. Yu, S. J. Jeon, J. Y. Choi, Y. W. Han, E. J. Ko, D. K. Moon, *Small* **2019**, *15*, 1805321.

[20] K.-S. Chen, H.-L. Yip, C. W. Schlenker, D. S. Ginger, A. K.-Y. Jen, *Org. Electron.* **2012**, *13*, 2870.

[21] C.-C. Chueh, K. Yao, H.-L. Yip, C.-Y. Chang, Y.-X. Xu, K.-S. Chen, C.-Z. Li, P. Liu, F. Huang, Y. Chen, W.-C. Chen, A. K.-Y. Jen, *Energy Environ. Sci.* **2013**, *6*, 3241.

[22] P.-T. Tsai, C.-Y. Tsai, C.-M. Wang, Y.-F. Chang, H.-F. Meng, Z.-K. Chen, H.-W. Lin, H.-W. Zan, S.-F. Horng, Y.-C. Lai, P. Yu, *Org. Electron.* **2014**, *15*, 893.

[23] S. Venkatesan, Q. Chen, E. C. Ngo, N. Adhikari, K. Nelson, A. Dubey, J. Sun, V. Bommisetty, C. Zhang, D. Galipeau, Q. Qiao, *Energy Technol.* **2014**, *2*, 269.

[24] B. R. Aïch, S. Beaupré, M. Leclerc, Y. Tao, *Org. Electron.* **2014**, *15*, 543.

[25] O. Synooka, K.-R. Eberhardt, H. Hoppe, *RSC Adv.* **2014**, *4*, 16681.

[26] D. Liu, Z. Wang, S. Zhang, Z. Zheng, B. Yang, W. Ma, J. Hou, *RSC Adv.* **2015**, *5*, 69567.

[27] G. Susanna, L. Salamandra, C. Ciceroni, F. Mura, T. M. Brown, A. Reale, M. Rossi, A. Di Carlo, F. Brunetti, *Sol. Energy Mater. Sol. Cells* **2015**, *134*, 194.

[28] F. Machui, S. Abbott, D. Waller, M. Koppe, C. J. Brabec, *Macromol. Chem. Phys.* **2011**, *212*, 2159.

[29] B. Walker, A. Tamayo, D. T. Duong, X.-D. Dang, C. Kim, J. Granstrom, T.-Q. Nguyen, *Adv. Energy Mater.* **2011**, *1*, 221.

[30] J. H. Hildebrand, R. L. Scott, *J. Chem. Phys.* **1952**, *20*, 1520.

[31] C. Hansen, *Hansen Solubility Parameters*, CRC Press, Boca Raton FL **2007**.

[32] D. T. Duong, B. Walker, J. Lin, C. Kim, J. Love, B. Purushothaman, J. E. Anthony, T.-Q. Nguyen, *J. Polym. Sci., Part B: Polym. Phys.* **2012**, *50*, 1405.

[33] N. Cho, H.-L. Yip, A. K.-Y. Jen, *Appl. Phys. Lett.* **2013**, *102*, 233903.

[34] J. G. Tait, T. Merckx, W. Li, C. Wong, R. Gehlhaar, D. Cheyns, M. Turbiez, P. Heremans, *Adv. Funct. Mater.* **2015**, *25*, 3393.

[35] F. Machui, S. Langner, X. Zhu, S. Abbott, C. J. Brabec, *Sol. Energy Mater. Sol. Cells* **2012**, *100*, 138.

[36] I. Burgués-Ceballos, F. Machui, J. Min, T. Ameri, M. M. Voigt, Y. N. Luponosov, S. A. Ponomarenko, P. D. Lacharmoise, M. Campoy-Quiles, C. J. Brabec, *Adv. Funct. Mater.* **2014**, *24*, 1449.

[37] R. Po, G. Bianchi, C. Carbonera, A. Pellegrino, *Macromolecules* **2015**, *48*, 453.

[38] M. Wakioka, N. Ichihara, Y. Kitano, F. Ozawa, *Macromolecules* **2014**, *47*, 626.

[39] A. S. Dudnik, T. J. Aldrich, N. D. Eastham, R. P. H. Chang, A. Facchetti, T. J. Marks, *J. Am. Chem. Soc.* **2016**, *138*, 15699.

[40] B. R. Aïch, J. Lu, S. Beaupré, M. Leclerc, Y. Tao, *Org. Electron.* **2012**, *13*, 1736.

[41] J. A. Bartelt, J. D. Douglas, W. R. Mateker, A. El Labban, C. J. Tassone, M. F. Toney, J. M. J. Fréchet, P. M. Beaujuge, M. D. McGehee, *Adv. Energy Mater.* **2014**, *4*, 1301733.

[42] A. A. Paraecattil, N. Banerji, *J. Am. Chem. Soc.* **2014**, *136*, 1472.

[43] Y. Zhu, Z. Chen, Y. Yang, P. Cai, J. Chen, Y. Li, W. Yang, J. Peng, Y. Cao, *Org. Electron.* **2015**, *23*, 193.

[44] M. Lamarche, M. T. Dang, J. Lefebvre, J. D. Wuest, S. Roorda, *ACS Sustain. Chem. Eng.* **2017**, *5*, 5994.

[45] N. P. Holmes, H. Munday, M. G. Barr, L. Thomsen, M. A. Marcus, A. L. D. Kilcoyne, A. Fahy, J. van Stam, P. C. Dastoor, E. Moons, *Green Chem.* **2019**, *21*, 5090.

[46] S. E. Shaheen, C. J. Brabec, N. S. Sariciftci, F. Padinger, T. Fromherz, J. C. Hummelen, *Appl. Phys. Lett.* **2001**, *78*, 841.

[47] H. Hoppe, M. Niggemann, C. Winder, J. Kraut, R. Hiesgen, A. Hinsch, D. Meissner, N. S. Sariciftci, *Adv. Funct. Mater.* **2004**, *14*, 1005.

[48] B. A. Collins, Z. Li, J. R. Tumbleston, E. Gann, C. R. McNeill, H. Ade, *Adv. Energy Mater.* **2013**, *3*, 1.

[49] D. Bartesaghi, M. Turbiez, L. J. A. Koster, *Org. Electron.* **2014**, *15*, 3191.

**ADVANCED
SCIENCE NEWS**

www.advancedsciencenews.com

**ADVANCED
ENERGY & SUSTAINABILITY
RESEARCH**
Open Access

www.advenergysustres.com

[50] S. Kouijzer, J. J. Michels, M. van den Berg, V. S. Gevaerts, M. Turbiez, M. M. Wienk, R. A. J. Janssen, *J. Am. Chem. Soc.* **2013**, *135*, 12057.

[51] A. B. Sieval, J. C. Hummelen, in *Organic Photovoltaics*, Wiley-VCH Verlag GmbH & Co. KGaA, Weinheim, Germany **2014**, pp. 209–238.

[52] J. K. Lee, W. L. Ma, C. J. Brabec, J. Yuen, J. S. Moon, J. Y. Kim, K. Lee, G. C. Bazan, A. J. Heeger, *J. Am. Chem. Soc.* **2008**, *130*, 3619.

[53] J. Peet, J. Y. Kim, N. E. Coates, W. L. Ma, D. Moses, A. J. Heeger, G. C. Bazan, *Nat. Mater.* **2007**, *6*, 497.

[54] L. Li, H. Tang, H. Wu, G. Lu, X. Yang, *Org. Electron.* **2009**, *10*, 1334.

[55] K. X. Steirer, M. O. Reese, B. L. Rupert, N. Kopidakis, D. C. Olson, R. T. Collins, D. S. Ginley, *Sol. Energy Mater. Sol. Cells* **2009**, *93*, 447.

[56] A. Lange, W. Schindler, M. Wegener, K. Fostiropoulos, S. Janietz, *Sol. Energy Mater. Sol. Cells* **2013**, *109*, 104.

[57] X. Guo, M. Zhang, C. Cui, J. Hou, Y. Li, *ACS Appl. Mater. Interfaces* **2014**, *6*, 8190.

[58] C. Sprau, F. Buss, M. Wagner, D. Landerer, M. Koppitz, A. Schulz, D. Bahro, W. Schabel, P. Scharfer, A. Colsmann, *Energy Environ. Sci.* **2015**, *8*, 2744.

[59] J. J. van Franeker, M. Turbiez, W. Li, M. M. Wienk, R. A. J. Janssen, *Nat. Commun.* **2015**, *6*, 6229.

[60] C.-D. Park, T. A. Fleetham, J. Li, B. D. Vogt, *Org. Electron.* **2011**, *12*, 1465.

[61] C.-D. Park, T. Fleetham, J. Li, *Org. Electron.* **2015**, *16*, 95.

[62] J. Griffin, A. J. Pearson, N. W. Scarratt, T. Wang, A. D. F. Dunbar, H. Yi, A. Iraqi, A. R. Buckley, D. G. Lidzey, *Org. Electron.* **2015**, *21*, 216.

[63] M. De Vincenzi, M. Silano, A. De Vincenzi, F. Maialetti, B. Scazzocchio, *Fitoterapia* **2002**, *73*, 269.

[64] OECD High Production Volume Chemicals Programme, "Benzaldehyde Screening Information Data Set", https://hpvchemicals.oecd.org/UI/handler.axd?id=cbba08a9-5eda-4930-92ad-540207d26a84 (accessed: April 2021).

[65] C. Piliego, T. W. Holcombe, J. D. Douglas, C. H. Woo, P. M. Beaujuge, J. M. J. Fréchet, *J. Am. Chem. Soc.* **2010**, *132*, 7595.